氷の自励振動成長—Ice Crystal 2 実験の成果—

○古川義純，長嶋剣，麻川明俊，中坪俊一，村田憲一郎，佐崎元（北大低温研），吉崎泉，田丸晴香（JAXA），島岡太郎（JSF），曽根武彦（JAMSS），真木孝雄，山本明日佳（オリンパス）

Self-Oscillatory Growth of Ice -Ice Crystal 2 Experiments-

○Yoshinori FURUKAWA, Ken NAGASHIMA, Harutoshi ASAKAWA, Shunichi NAKATSUBO, Kenichiro MURATA, Gen SAZAKI (Hokkaido Univ.), Izumi YOSHIZAKI, Haruka TAMARU (JAXA), Taro SHIMAOKA (JSF), Takehiko SONE (JAMSS), Takao MAKI, Asuka YAMAMOTO (Olympus)

1. Introduction

Ice Crystal 2 experiments were conducted in KIBO of ISS. Free growth of ice crystals in a supercooled bulk water containing a small amount of antifreeze glycoprotein (AFGP), which was a functional biomaterial to inhibit the freezing of fish body under the sub-zero temperature condition, was observed in-situ using a newly-developed optical system. Experiments were repeated more than originally intended repeat count in the period from November 2013 to June 2014. Ice crystal growth were successfully observed and clear interference fringes were obtained on the ice(basal)/water interfaces. We describe an overview of experimental results in this presentation.

2. Experimental Procedures

The experimental cartridge, which was newly developed for this experiment, was composed of two parts, as was the cartridge used for first space experiment[1], but the two parts were extensively modified for the second experiment. For the growth apparatus of an ice crystal, a spherical growth cell (40 mm in diameter) was made and it was equipped with the rotating mechanism of a glass capillary around its axis. As the optical system to observe ice crystal growth, a Michelson-type interference microscope combined with a phase contrast microscope was installed in the cartridge. These systems allow observation of step migrations on the growing basal face and measurement of growth velocity at the same time.

The cartridge was transported to the ISS in August 2013 and the first experiments were started at the end of this month. However, our experiment fell into difficulties in the power supply system immediately after starting experiments. Fortunately, experiments could be started again after troubleshooting, and for the last time 124 growth experiments were carried out in space under various supercooling conditions in the range between 0.1 and 1 K. Ice crystal growth was observed in almost every experiment, and interference fringes on the basal faces were successfully observed in more than 20% of the experiments.

3. Experimental Results

Time fluctuation of growth rate for the prism face of an ice crystal in the AFGP solution was first observed in one-directional growth experiments conducted in a thin growth cell with no convection in the cell[2]. Zepeda et al.[3,4] directly observed that the prism faces for which growth had been stopped by adsorption of AFGP molecules started to grow again along with desorption of AFGP molecules from the interface. These observations indicate that the growth velocities of prism faces should not be constant but fluctuate with growth time. This kind of fluctuation may give suggestions for the self-oscillatory growth of a prism face.

In the present space experiments, clear interference fringes were observed on the basal faces of growing ice crystals. Furthermore we observed the fluctuation of fringe migrations. We can estimate the growth rates of basal faces by analyzing the movement of interference fringes observed. Consequently, this experimental result means that the growth rate of a basal face fluctuates with the growth time under the microgravity condition in which the disturbances like thermal convection were completely taken out.

The mechanism for the self-oscillations of growth rates should be explained in relation to the adsorption-desorption processes of AFGP molecules on the growing interfaces. Consequently, the experimental data obtained in space will provide direct information about why adsorption and desorption can occur periodically on both prism and basal interfaces of an ice crystal. Such information is expected to contribute to elucidation of the mechanism of the antifreeze effect.

References

1) E. Yokoyama, I. Yoshizaki, T. Shimaoka, T. Sone, T. Kiyota and Y. Furukawa: J. Phys. Chem., **B115** (2011) 8739.

2) Y. Furukawa, N. Inohara and E. Yokoyama: J. Cryst. Growth, **275** (2005) 167.

3) S. Zepeda, E. Yokoyama, Y. Uda, C. Katagiri and Y. Furukawa: Cryst. Growth Des., **8** (2008) 3666.

4) S. Zepeda, Y. Uda and Y. Furukawa: J. Jpn. Asso. Cryst. Growth, **35** (2008) 151.

微小重力環境下で **TLZ** 法により成長した **SiGe** 結晶内組成分布の数値解析

○住岡沙羅，阿部敬太，杉岡健一，久保正樹，塚田隆夫（東北大院工），

木下恭一，荒井康智，稲富裕光（宇宙航空研究開発機構）

Numerical Study on the Composition Distributions in SiGe Crystals Grown by TLZ Method under Microgravity

○Sara SUMIOKA, Keita ABE, Ken-ichi SUGIOKA, Masaki KUBO, Takao TSUKADA (Tohoku Univ.),

Kyoichi KINOSHITA, Yasutomo ARAI, Yuko INATOMI (JAXA)

1. Introduction

The second microgravity experiment on SiGe crystal growth by the traveling liquidus-zone (TLZ) method has been carried out aboard the Japanese Experiment Module "Kibo" in the International Space Station in July 2013[1]. In this work, we numerically investigated the transport phenomena and solidification taking place in this microgravity experiment in detail, using a mathematical model developed by the present authors[2]. Particularly, the axial and radial composition distributions of Ge in the crystal were discussed, comparing the numerical results with the experimental ones.

2. Mathematical model

The axisymmetric model used here can predict the temperature distributions in the BN crucible, Si seed, Si feed, SiGe melt and crystal, the composition distributions of Ge in the melt, and the shapes of the melt/SiGe crystal and melt/Si feed in **Fig.1**, using the finite difference method on the basis of boundary-fitted coordinate transformation[2]. The temperature at the outer wall of the BN crucible was determined by a global heat transfer analysis in a gradient heating furnace used in the microgravity experiment, using FLUENT 12.1.

3. Results and discussion

Figure 2 shows the numerical and experimental results of the axial composition distributions of Ge along the central axis of the grown crystal. Both the composition distributions show the U-shaped one at the early to middle stage of the growth, but finally become constant. The origin of such a U-shaped distribution was considered to be the emissivity change of the cartridge surface, in which the BN crucible in **Fig.1** is included, due to oxidization, similarly to the first microgravity experiment[3].

Figure 3 shows the numerical and experimental results of the radial composition distributions of Ge at the growth lengths of (a) 4.0 and (b) 7.5 mm in **Fig.2**. From the figure, it is found that the mean values of Ge compositions depend on the growth length, whereas the radial distributions are kept relatively uniform throughout the entire crystal.

References

1) K. Kinoshita, Y. Arai, T. Tsukada, Y. Inatomi, H. Miyata, and R. Tanaka, *J. Cryst. Growth* (Submitted)

2) K. Abe, S. Sumioka, K. Sugioka, M. Kubo, T. Tsukada, K. Kinoshita, Y. Arai, and Y. Inatomi, *J. Cryst. Growth*, **402** (2014) 71

3) K. Kinoshita, Y. Arai, Y. Inatomi, T. Tsukada, S. Adachi, H. Miyata, R. Tanaka, J. Yoshikawa, T. Kihara, H. Tomioka, H. Shibayama, Y. Kubota, Y. Warashina, Y. Sasaki, Y. Ishizuka, Y. Harada, S. Wada, C. Harada, T. Ito, M. Takayanagi, and S. Yoda, *J. Cryst. Growth*, **388** (2014) 12
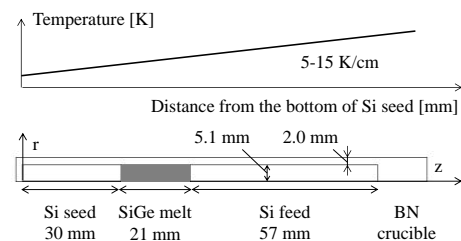
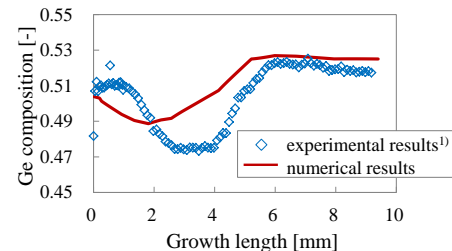**Fig. 1** Schematic diagram of TLZ method

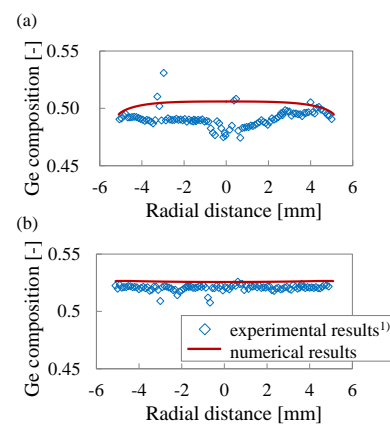**Fig.2** Axial composition distributions of Ge in SiGe crystals

Fig.3 Radial composition distributions of Ge in SiGe crystals (a) growth length: 4.0 mm, (b)7.5 mm

微小重力下における TLZ 法による均一組成 SiGe 結晶育成の研究（その 2）

○木下恭一 [1]，荒井康智 [1]，稲富裕光 [1]，塚田隆夫 [2]，宮田浩旭 [3]，田中涼太 [3]，阿部敬太 [2]，住岡沙羅 [2]

（1::宇宙航空研究開発機構，2:東北大学大学院工学研究科，3:（株）エイ・イー・エス）

Growth of Homogeneous SiGe Crystals by the TLZ Method in Microgravity (Report-2)

○K. KINOSHITA[1], Y. ARAI[1], Y. INATOM[1], T. TSUKADA[2], H. MIYATA[3], R. TANAKA[3], K. ABE[2],
S. SUMIOKA[2] (1: Japan Aerospace Exploration Agency, 2: Dept. Chem. Eng. Tohoku Univ., 3: AES Co. Ltd.)

1. Introduction

SiGe crystal growth experiments aboard the "Kibo" in the ISS were carried out for evaluating the growth model of the traveling liquidus-zone (TLZ) method. Results of three experiments are summarized along with the growth conditions.

2. Experiments

10 mm diameter $Si_{1-x}Ge_x$ (x ~ 0.5) crystals were grown by the TLZ methods. Orientation of the Si seed was <100>. The zone former Ge was polycrystalline. After removing the surface contamination and the oxide layer by etching in an acid solution, a 30 mm long Si seed, a 20 mm long Ge zone forming material and a 57 mm long Si feed were put into a boron nitride (BN) crucible with a carbon spring for avoiding free melt surface. The crucible was vacuum sealed in a quartz ampoule at about 1×10^{-5} Pa. The ampoule wrapped by ZrO_2 cloth was then inserted into a metal cartridge. The assembled metal cartridges were heated in the gradient heating furnace. Growth conditions are as follows, temperature gradient: 9℃/cm, heater translation rate 0.1 mm/h, freezing interface temperature: 1107℃, experiment period: 72～124 h. In the second and third experiments, heater temperatures were adjusted so as to cancel the oxidation effect of the cartridge surface. The returned samples were analyzed by an electron probe microanalyzer and by an electron backscatter diffraction after cutting parallel to the growth axis and polishing.

3. Results and discussion

The outer view of a sample obtained in the third experiment is shown in Fig. 1. A seed, SiGe crystal region, quenched melt and a Si feed are indicated in the figure. No missing part, large voids and major cracks were detected in a cross section of the grown crystal. No free surface of the melt would be existed during the experiment since a trace of flown melt which was pushed by a carbon spring toward the seed was observed on the feed surface. Marangoni convection would, therefore, be suppressed in the experiment.

The axial Ge concentration profile is shown in Fig. 2. Average Ge concentration was 49.0±2 at% and a dip of Ge concentration was observed. It is shown that the dip is related to temperature rise in the cartridge due to emissivity change of the cartridge surface by oxidation[1]. Therefore, heater temperatures were adjusted to cancel the emissivity change but the effect of emissivity change was not canceled. The results implied that timing of heater temperature adjustment did not coincide with the timing of the emissivity change. Emissivity change may depend not only on heating period but also on the level of vacuum in the furnace chamber. Then, timing of heater temperature change to cancel the emissivity change is very difficult. Cartridges with oxidized surface may be useful to avoid this effect.

Growth length was observed to be 14.5 mm, which is comparable to the expected length of 15 mm. Growth interface shape was observed by the striation[2] which was caused by step temperature changes of 1℃. At the seed/crystal interface, it was convex toward the melt. The seed/crystal interface shape may be resulted by the melt flow around the seed through a gap between the seed and the crucible wall at the start of the crystal growth. The interface gradually changed to a flat shape according as the crystal growth proceeded. This tendency was similar to the second sample, but the radial compositional homogeneity was better in the third experiment since the interface curvature is less than the second experiment. In the presentation, results of three experiments will be compared and discussed.
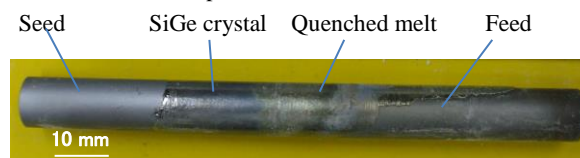

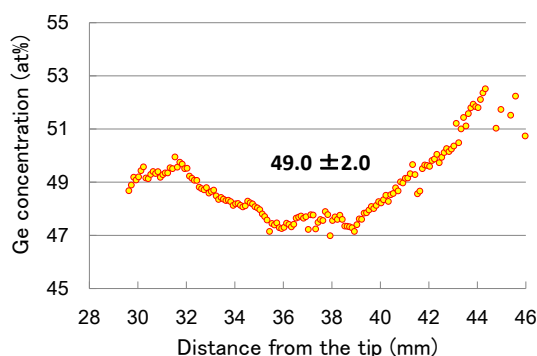**Fig. 1.** Outer view of a sample of the third experiment.

Fig. 2. Ge concentration profile along the growth axis.

References

1) K. Abe *et al*., J. Crystal Growth **402** (2014) 71.
2) Y. Arai *et al*., NCCG-44 予稿 (2014).

観測ロケットで得られる微小重力環境下での気相からの均質核生成の"その場"観察実験

○木村勇気，田中今日子（北大），塚本勝男（東北大・大阪大），竹内伸介，稲富裕光（JAXA）

In-situ Observation of Homogeneous Nucleation from Vapor Phase under
Microgravity Prepared by a Sounding Rocket

○Yuki KIMURA, Kyoko K. TANAKA (Hokkaido Univ.), Katsuo TSUKAMOTO (Tohoku Univ, Osaka Univ.), Shinsuke TAKEUCHI, Yuko INATOMI (JAXA)

1. Introduction

It is difficult to find homogeneous nucleation event on the Earth because there are lots of heterogeneous nucleation site. In case of a nucleation event around dying star, there is almost no solid materials available for heterogeneous nucleation site and, therefore, homogeneous nucleation govern the properties of cosmic dust, which is produced from a supercooled gas in outflow from dying stars or in a gas plume after shock wave heating in the primitive solar nebula. To know the formation process of cosmic dust particles via homogeneous nucleation, we have to obtain the physical parameters, especially surface free energy and sticking probability, of nanometer sized particles, because of the size of cosmic dust is typically less than 100 nm. To determine the physical parameters of nanoparticles, we developed an in-situ observation system of temperature and concentration during homogeneous nucleation in vapor phase using interferometry.

2. Benefits of microgravity experiment

We produce nanoparticles from a supercooled vapor after evaporation of a selected material by electrical heating in a gas atmosphere in the laboratory. Using the interferometry, surface free energy and sticking probability of manganese nanoparticle were determined from timescale for gas cooling and condensation temperature based on nucleation theories [1]. However, in case of 1 G, convection of gas atmosphere caused by thermal heating of an evaporation source generates heterogeneity of nucleation environment. In addition, there is a higher possibility of that number density of nuclei decreases by fusion growth by collide each other after a stage of nucleation [2]. This fusion growth may be one of reasons of large differences of nucleation rates between experiments and theories. Microgravity environment will resolve these difficulties of 1 G experiments. Large difference of reported sticking probabilities obtained by microgravity (~10^{-5}) [3] and 1 G (~1) [4] is also give us a motivation to do microgravity experiment.

If same kinds of experiments are performed in microgravity, evaporated vapor will diffuse uniformly and the temperature profile will become concentric around the evaporation source. As the result, nucleation will occur at the same condition, i.e., same supersaturation. Then, we can obtain physical properties of nanoparticles more precisely. Therefore, we performed a microgravity experiment using the sounding rocket S-520-28.

3. Experimental procedure

We prepared specially designed three experimental systems, named DUST 1 to 3, with almost same configuration except evaporation source and gas pressure in the chamber were installed into the rocket. The each system has a double wavelength Mach–Zehnder-type interferometer with a working chamber and a camera recording system on an aluminum base plate. The evaporation source and gas atmosphere of each system are tungsten without iron and a gas mixture of oxygen (4.0×10^3 Pa) and argon (3.6×10^4 Pa) for DUST 1, iron and argon (2.0×10^4 Pa) for DUST 2, and iron and argon (4.0×10^4 Pa) for DUST 3. Argon gas works as a buffer gas to shorten the mean free path of evaporated vapor. Evaporated vapor of tungsten oxide or iron was diffused, cooled and nucleated in the gas atmosphere. Changes in refractive index are induced not only by variations in temperature, but also by variations in the concentration of iron vapor. Because the Mach–Zehnder-type interferometer has two lasers of polarized green and red, the temperature and concentration could be determined simultaneously from a movement of the interference fringes.

4. Results and discussion

Using a specific timescale for gas cools, we calculated the equations governing the time evolution of the gas number density of Fe atoms and the nucleation rate. From the comparisons between the numerical simulations and the experimental results, we can determine the sticking probability for Fe. Then, we obtain the nucleation temperatures, which have very large supercooling larger than 1000 K, and sticking probability as small as 10^{-4} for iron.

References

1) Y. Kimura, K. K. Tanaka, H. Miura, K. Tsukamoto, Crystal Growth & Design, **12** (2012) 3278.

2) Y. Kimura, In: Nanodust in the Solar System: Discoveries and Interpretations. Eds. Ingrid Mann, Nicole Meyer-Vernet, Andrzej Czechowski, Springer-Verlag (2012) p. 31-46.

3) B. P. Michael, J. A. Nuth III, L. U.Lilleleht, The Astrophysical Journal, **590** (2003) 579.

4) S. Tachibana, H. Nagahara, K. Ozawa, Y. Ikeda, R. Nomura, K. Tatsumi, Y. Joh, The Astrophysical Journal, 736 (2011) 16.

NanoStep プロジェクトから得たもの

○塚本勝男（東北大）, 鈴木良尚（徳島大）, 三浦均（名市大）, 吉崎泉（JAXA）

What we have learned from the NanoStep project

○Katsuo TSUKAMOTO (Tohoku Univ.), Yoshihisa SUZUKI (Tokushima Uni.),

Hitoshi MIURA (Nagoya City Univ.), Izumi YOSHIZAKI (JAXA)

We have been interested in the growth mechanism of lysozyme crystals under microgravity. This is because for many years perfection of space grown crystals claimed to be better than earth grown crystals. However there are also many cases showing opposite results. To clarify the factors controlling the perfection, we started NanoStep Project employing in-situ observation method of crystal growth, in which growth rate vs supersaturation has successfully been measured for the first time through observation of the surface features were also observed by laser interferometry in Kibo in 2012 [1]. The former rate measurement and the latter observation of surface features are important respectively for the analysis of growth kinetics and for the study of effect of impurity adsorption and effect of concentration inhomogeneity around a crystal.

The experiments finished successfully but the results obtained from NanoStep project were much better than the expectation from ground-based experiments. We therefore had to repeat more reference experiments later on for the comparison.

The results are summarized:

(1) The growth rate in spiral growth regime under microgravity is higher than that in gravity if we compare the growth rate of crystals from the same purity solutions. The growth regime has usually been used to grow protein crystals for structural analysis.

(2) The difference of the growth rate is attributed to the anisotropic adsorption of dimer impurities along growth steps parallel to the <1-11> and the <-111> directions, the former of which is nearly equal in the macro-bond strength [2] to the latter but molecular arrangement at each step fronts is different. As long as we do experiment in gravity, crystals experience stronger effect of impurity effect. Probably this improved effect would be valid only for these impurities with larger diameter than protein molecules.

(3) Supersaturation distribution over growing crystal surface was unexpectedly more homogeneous in microgravity leading to much less supersaturation decrease if measured from the edge to the middle of the crystal surface. This would give rise to the improved stability of crystal face, which possibly results in the improved perfection of crystals.

(4) Some other unexpected results were obtained: effect of cooperation spiral growth on the growth rate and slope of spiral hillocks, dislocation nucleation at the seed crystal surface and so on.

These experimental results show that Kibo becomes a real laboratory in which we can run experiments in the same or even better conditions so that we can perform high level experiments as we do in our laboratories on the ground.

[1] I. Yoshizaki, K. Tsukamoto, T. Yamazaki, K. Murayama, K. Oshi, S. Fukuyama, T. Shimaoka, Y. Suzuki, M. Tachibana, Growth rate measurements of lysozyme crystals under microgravity conditions by laser interferometry, Review of Scientific Instruments, 84 (2013).

[2] Y. Matsuura, A.A. Chernov, Morphology and the strength of intermolecular contacts in protein crystals, Acta crystallographica. Section D, Biological crystallography, 59 (2003) 1347-1356.

地上と無重力での結晶表面の二次元過飽和度および成長速度分布の測定

〇村山健太（名古屋大），塚本勝男（東北大），横山悦郎（学習院大）

Measurement of the Growth Rate and Supersaturation Distribution at the Crystal Surface on the Ground and Microgravity

〇Kenta MURAYAMA (Nagoya Univ.), Katsuo TSUKAMOTO (Tohoku Univ.),

Etsuro YOKOYAMA (Gakushuin Univ.)

1. Introduction

The convection in solution is restrained in microgravity environment so that the solute concentration is decreasing towards the crystal-solution interface because the crystal consumes solute in the solution as it grows (Berg effect). On the other hand, the convection disturbs the concentration field around the crystal on the ground. Therefore, the mechanism of the crystal growth on the ground and in microgravity should be different. To discuss this problem, direct measuring of the concentration filed and growth rate is very important. However, there is no direct observation of the relationship between growth rate and concentration field in microgravity or on the ground.

2. Experiments

We carried out the microgravity experiment in the International Space Station (ISS) that gives ideal environment without convection. A protein crystal grows within the cell whose temperature is controlled.

The "in-situ" observation of the concentration field around the crystal and the measurement of the growth rate of (110) surface were carried out by using the Mach-Zehnder and the Linnik interferometer, simultaneously. The sample used for the experiment is a tetragonal lysozyme (solution concentration 30 mg/ml, 50 mM Acetic acid buffer pH4.5, NaCl 2.5%). The crystal growth cell was conveyed to ISS after enclosing a seed crystal and solution on the ground. A seed crystal is put on the wall so that (110) surface becomes perpendicular to the optical path of the Linnik interferometer. Changing the temperature of solution performs the variation of the supersaturation of solution.

Same experiment on the ground was carried out to see the effect of the convection in solution.

3. Results and discussion

There is a large difference (about 16%) of the supersaturation between the central and the edge on the ground, mainly because of the convection plume of solutal convection. As a result, almost twice as large growth rate arises at the edges of the (110) surface as compared with the rate at the middle of the face, and thus flat crystal face cannot be maintained, leading to the instability of the face.

In microgravity, convection is suppressed and the supersaturation gradient along the surface was expected larger. However the supersaturation difference was for the first time measured to be very small (only about 2.4%) compared with that of under gravity. Normal growth rate distribution is almost uniform on the crystal surface in microgravity so that flat crystal face can be maintained.

According to this result, the upward flow due to the convection has the stronger influence than the Berg effect on the stability of a crystal surface.
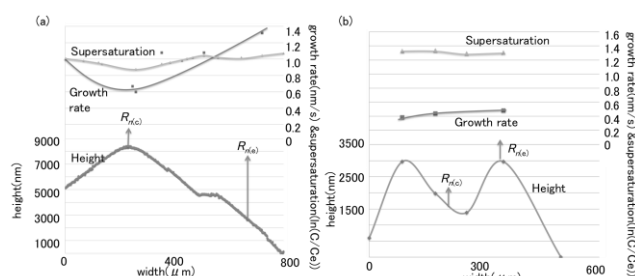

Fig.1 The topography plot of crystal surface, the distribution of the surface supersaturation and growth rate (a) on the ground and (b) in microgravity.
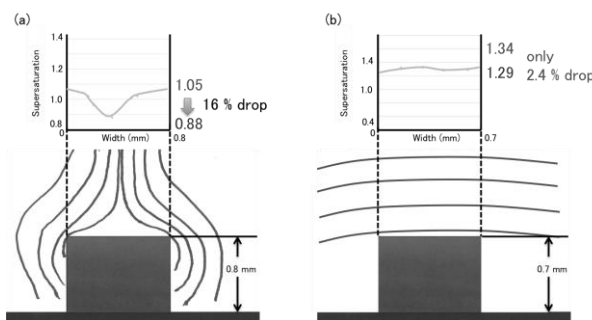

Fig.2 Supersaturation distribution above the (110) face of the lysozyme crystal (a) on the ground (b) in microgravity.

References

1) W. F. Berg: Proc. R. Soc. Lond. A, **164** (1938) 79.

2) E. Yokoyama and T. Kuroda: Phys. Rev. A, **41** (1990) 2038.

3) F. Bedarida: J. Cryst. Growth, **79** (1986) 43.

4) K. Onuma, K. Tsukamoto and I. Sunagawa: J. Cryst. Growth, **89** (1988) 177.

5) K. Murayama, Katsuo Tsukamoto, Atul Srivastava, Hitoshi Miura, Etsuro Yokoyama, and Yuki Kimura: Cryst. Res. Technol., **49** (2014) 315.

宇宙実験を利用した実用 X 線構造解析向けタンパク質結晶化実験の 30 年とこれから

田仲 広明（（株）コンフォーカルサイエンス）

A Historical Perspective on Protein Crystallization in Space for Practical X-ray Structural Analysis over the Past 30 years and Towards the Future

Hiroaki TANAKA (Confocal Science Inc.)

1. Space Experiment of NASA and ESA in the past

The first successful protein crystallization growth (PCG) experiment in microgravity was performed in Spacelab by Littke et al. [1] in 1983. Since then, many PCG experiments in microgravity have been performed by NASA, ESA, RSA, JAXA (NASDA) etc., but the impact of microgravity crystallization on structural biology was not established for a long time. NASA performed protein crystallization experiment for X-ray diffraction analysis almost once in twice during 1990s. But in 2000, the National Research Council of the United States reported that the impact of microgravity crystallization on structural biology as a whole is extremely limited, and NASA stopped protein crystallization experiment until recently. ESA performed space experiment almost once a year during 1990s and experimentally studied the effects of microgravity on protein crystal growth. From these activities,, certain mechanisms for the improvement of crystal quality were reported[2,3,4].

2. Space Experiment of JAXA in the past and present

JAXA/NASDA has been conducting the protein crystallization experiment in microgravity environment since 1992 (FMPT (STS-47)). In 1997, 15 protein samples were launched to space (STS-84). Through these experiences, it was realized that specific crystallization techniques for microgravity environment were mandatory. From 2002 to present, JAXA conducted GCF, NGCF and PCG project to provide PCG experiments for X-ray diffraction analysis combined with many technological developments. During these projects, we found that the biggest advantage of the PCG in microgravity is to improve the maximum resolution of the crystals far beyond what can be obtained from the terrestrially-grown best crystals[5]. Simultaneously, the following concerns were arisen.

▪ In the laboratory, even if the protein sample is not so stable, we may obtain a crystal suitable for X-ray diffraction experiment. But for the space experiment, since it takes longer from the launch to the recovery, the deterioration of the protein sample may cause a difficulty of crystal growth.

▪ In the laboratory, even if the possibility of the crystal growth is low, we may obtain a crystal suitable for X-ray diffraction experiment. But for the space experiment, it may end up with no crystal growth.

▪ In the laboratory, researchers usually use a vapor-diffusion method for crystallization. But for the space experiment, it may be better to use a liquid-liquid diffusion method to avoid Marangoni convection. So, we have to acquire techniques for the optimization of crystallization conditions and for handling crystals, specialized for that method.

▪ It is said that microgravity effects on growing crystal is due to the formation of protein and impurity depletion zones around the growing crystal. Therefore the crystallization condition which enhances these effects is favorable[6,7]. However for most of the researchers, it is not necessary to pay attention to this kind of matter on the ground. So we have to make efforts to explain how important it is to optimize crystallization condition suitable for space experiment.

Considering these problems, we have extensively supported researchers from a proposal submission to X-ray diffraction data collection. As a result, more effective usage of the microgravity environment for crystallization has come true. So far, JAXA space experiment has contributed to the structure analysis of almost 20 kinds of protein, resulting in the publication of paper and PDB registration. Therefore, we believe that the reputation of the PCG experiment in microgravity has been favorably changing.

3. Space Experiment in the future

The technique for protein crystallization experiment in space is still developing; a crystallization condition optimization method customized for each protein's property; a crystallization cell suitable for growing large crystals for neutron diffraction experiment, etc. Some of the accumulated knowledge by technical development for the space experiment so far can be applied to the crystallization experiment in the laboratory. We strongly convince that PCG in space is the final method to improve the maximum resolution of the protein crystals, which will contribute to the sub-Å structure analysis.

References

1) W. Littke, C. J. John: Science **225** (1984) 203.

2) N. E. Chayen et al.: J. Crystal Growth 171 (1997) 219.

3) F. Otálora et al.: Acta Cryst. **D57** (2001) 412.

4) B. R. Thomas et al.: J. Cryst. Growth **211** (2000) 149.

5) S. Takahashi et al.: J Synchrotron Rad.. **20** (2013) 968.

6) H. Tanaka et al.: Ann. N.Y. Acad. Sci. **1027** (2004) 10.

7) H. Tanaka et al.: J. Synchrotron Rad. **20** (2013) 1003.

ISS きぼう船内実験室利用テーマ「Soret-Facet」の運用状況

○鈴木進補，橋本栄尭，長田拓真，森雄飛（早大），稲富裕光（ISAS），正木匡彦（芝浦工大），
渡邉匡人，水野章敏（学習院大），上野一郎（東理大），山根岳志（富山大），伊丹俊夫（北大），
中村裕広，勝田真登，伊藤裕一，大熊隼人（JAXA），島岡太郎（JSF），曽根武彦（JAMSS）

Current status of "Soret-Facet" experiments aboard the ISS-JEM

○S.Suzuki, Y.Hashimoto, T.Osada, Y.Mori (Waseda univ.), Y.Inatomi (ISAS), T.Masaki (Shibaura Inst. Tech.),
M.Watanabe, A.Mizuno (Gakushuin Univ.), I.Ueno (Tokyo Univ. Sci.), T.Yamane (Toyama Univ.), T.Itami
(Hokkaido Univ.), Y,Nakamura, M.Katsuta, Y.Ito, H.Ohkuma (JAXA), T.Shimaoka (JSF), T.Sone (JAMSS)

1. Introduction

Accurate data and basic knowledge of Soret coefficient S_T are necessary for the discussion on the process where temperature gradient exists, such as crystal growth, solidification and so on. We started the experiments "*Soret-Facet*"[1] on July 2, 2014 to obtain accurate data of S_T under microgravity conditions in the Japanese Experiment Module (JEM, Kibo) in the International Space Station (ISS). The concentration and temperature changes were measured in a solution under a temperature gradient using two-wavelength Mach-Zehnder interferometer. The almost half of the planned experiments were completed. We report the overview and current status of the experiments in ISS/JEM.

2. Overview of the Experiments

The *FACET-cells* and two-wavelength Mach-Zehnder interferometer in the Solution Crystallization Observation Facility (SCOF) were used. There were two *FACET-cells* (Cell 1 and 2). The *FACET-cells m*ade of quartz glass were filled with a solution of Salol and *tert*-butyl alcohol. The nominal concentration of the *tert*-butyl alcohol was 3 mol% (Cell 1) and 6 mol% (Cell 2). Only the experiments of Cell 1 were performed until September 2014. The apparatus and the solution specimen were identical to those used in the experiments "*FACET*", which were former ISS/JEM experiments for observation of crystal growth. Therefore, the "*Soret-Facet*" experiments were able to be performed without launching apparatus and specimen.

The *FACET-cell* (interior dimensions 16^Lx4.8^Wx1^T mm^3) was sandwiched with two Peltier devices for controlling the temperature. Laser beams (λ=532 and 780 nm) were applied to the solution in the Mach-Zehnder interferometer. Interference fringes were recorded during the experiments. The change and distribution of temperature and concentration were calculated from the moving distances of the interference fringes generated by each laser beam. The shift of the fringes generated by thermal expansion of the glass cell was canceled by the moving distance of the fringes of the cell wall[2].

The following experiments were performed by varying the temperature programs.

 (a) *Melting Point*: The temperature was controlled so as to set the solid-liquid interface in the middle position between two thermo-couples. This was done to estimate the concentration of *tert*-butyl alcohol, which was set before the launch and might have changed during long time proceeded.

(b) *Solid/Liquid Soret*: The temperature distribution was set so that the solution is solid in the colder side and liquid in the hotter side to discuss the Soret effect in a solid-liquid coexisting system.

(c) *Liquid Soret*: The specimen was melted completely. Then a temperature gradient was set by lowering the temperature of one side. The moving distance of the interference fringes was measured during the temperature and concentration change. The values of S_T were obtained through calculation of the temperature and concentration gradients in the stable state using the moving distance. The setting temperature gradient was varied in the range between 0.4 and 2 K/mm, and the setting temperature was varied in the range between 30 and 55 °C, including supercooled liquid temperature region.

(d) *Diffusion*: After the procedure of a "Liquid Soret" experiment, the temperature of the colder side was heated so that the temperature should be homogeneous in the solution. The moving distance of the fringes was measured during the transient phase from the state with a temperature gradient to the state with homogeneous temperature distribution.

3. Current Status and Trouble Shootings

All planed experiments of using "*Cell 1*" were performed in Kibo. Several unexpected problem arose during these experiments. The status and solution are as follows.

(1) Resolution of fringes: The *FACET-cell* allowed only a narrow cell wall to observe for the cancelation of the thermal expansion of the glass cell. Therefore, lateral interference fringes (aligned vertically to the temperature gradient) were applied. Before the µg experiments, it was confirmed that the lateral fringes provide the almost same S_T values as parallel fringes (aligned parallel to the temperature gradient), which have been used in 1g experiments.

(2) Hopping of interference fringes: Sudden hopping of interference fringes was found during experiments. As the hopping took place at the same time also in the glass cell, it was confirmed that the effect can be eliminated by cancelation procedure of thermal expansion of the glass cell.

(3) Gas bubbles: Since several gas bubbles were found in the solution especially in the solid/liquid Soret experiments, the observation window was set at a position away from the gas bubble. The effect of the bubble on the measurement is considered not to be significant, because there was no clear distortion of fringes around the gas bubble.

(4) Data loss: Movie images were disturbed by block noises possibly caused by single event of IPU (Image Processing Unit) in an experiment run. Two experiments of *Liquid Soret* were either aborted or performed with data loss due to a failure of Microgravity Measurement Apparatus (MMA). Another run for these experiments was performed without data loss later.

All of movie data of the planned experiments were acquired and currently under analysis.

References

1) S. Suzuki, *et al*., JASMAC27Abstructs (2013) 30.
2) Y. Mori, *et al*., Transactions of the JSASS, in press.

「きぼう」を利用した液柱マランゴニ対流実験

○松本聡（宇宙航空研究開発機構）

Overview of Experiment on Marangoni Convection in Liquid Bridge using Japanese Experiment Module KIBO

○Satoshi MATSUMOTO (JAXA)

1. Introduction

Instability problems in fluid dynamics is a research area where is being carried out actively. Fluid behavior sometimes shows a very interesting phenomenon because of its strong nonlinearity. Therefore, studying the instability problem might advance theoretical and mathematical science as well as fluid dynamics as to progress the concept of chaos.

Marangoni flow is categorized in the natural convection same as buoyancy convection caused by density difference. A trait of Marangoni convection is a surface-tension-driven flow which driving force is localized at the only surface. Of cause, the flow instability occurs in Marangoni convection like a hydrodynamics or hydrothermal instability[1].

Numerous studies have been carried out to make clear the instability in Marangoni convection. Two types of configuration were mainly focused, one was annular pool, other liquid bridge (cylindrical liquid column). The liquid bridge configuration simulates the floating-zone method for crystal growth such as semiconductor and oxide materials.

The final goal of JAXA Marangoni project is to fully understand Marangoni convection occurred in wide range of Prandtl number (Pr) fluid. For low and moderate Pr fluid, ground-based studies are performed[2-4].

For high Pr fluid, a liquid bridge of silicone oil is formed into a pair of supporting solid disks. The convection is induced by imposing the temperature difference between disks, one end heating and other end cooling. Due to the convective instability, flow transits from laminar to oscillatory, chaos, and turbulence flows one by ones as the driving force increases. We observe the flow and temperature fields in each stage and investigate the flow transition conditions and processes.

Overview of Marangoni experiment onboard the ISS is described in this paper.

2. Space experiment

One of the major advantages of the International Space Station (ISS) includes the long durational and high quality microgravity condition. A lot of experiments are carrying out utilizing such advantage. In fluid science field, Marangoni convection (thermocapillary convection) induced in half-zone liquid bridge have been observing both on the ground and on board the ISS. Japan Aerospace Exploration Agency (JAXA) implements space experiment on Marangoni convection with high Prandtl number. There are four experiments. The first experiment which principal investigator is Prof. Kawamura in Tokyo University of Science had started in 2008. After five years at present, eight series of experiments are completed and a plenty of fruitful results are obtained.

Fundamental questions regarding to Marangoni Convection are the mechanism of oscillatory flow onset and flow transition process. Four space experiments are implemented to solve above question utilized long durational microgravity condition.

Marangoni space experiment is performed using Fluid Physics Experiment Facility on Ryutai Rack in KIBO. Silicone oil is employed as a working fluid.

3. Perspectives

As expected, the measured critical temperature difference ΔT_c for the more viscous liquid is substantially higher than that for the less viscous one. Some of the experimental results are in good agreement with each other, while others show the similar patterns but are distinctly offset due, perhaps, to different fluid viscosity and the relative size of the liquid bridges[5,6]. JAXA will perform Marangoni experiments in KIBO until 2017. Through a series of the experiments, we will be able to systematically understand convective instability of Marangoni convection and make clear the universality and differences among convection such as unstable Rayleigh-Bénard convection or Taylor-Couette vortex flow.

References

1) S. Chandrasekhar: Hydrodynamic and Hydromagnetic Stability, Oxford University Press (1961)
2) K. Li, N. Imaishi, C.J. Jing, S. Yoda: J. Crystal Growth, **370**, (2007) 155
3) S. Matsumoto, H. Hayashida, H. Natsui, S. Yoda, N. Imaishi: Thermal Sci. and Eng., **12** (2004) 21
4) S. Simic-Stefani, M. Kawaji, S. Yoda: Int. J. Heat Mass Transfer, **49** (2006) 3167
5) H. Kawamura K. Nishino, S. Matsumoto, I. Ueno: J. Heat Transfer, **134** (2012) 031005
6) S. Matsumoto, K. Nishino, I. Ueno, T. Yano, H. Kawamura: Int. J. Microgravity Sci., 31 Suppl. (2014) S51

高プラントル数長液柱において表面張力流と逆向きに伝播する渦構造

○矢野大志，西野耕一（横浜国立大学），上野一郎（東京理科大学），松本聡（JAXA）

Traveling of Vortical Structure in the Direction Opposite to the Thermocapillary Flow in High Prandtl Number Long Liquid Bridge

○Taishi YANO, Koichi NISHINO (Yokohama National Univ.), Ichiro UENO (Tokyo Univ. of Science),

Satoshi MATSUMOTO (JAXA)

1. Introduction

The instability of thermocapillary convection in an infinite liquid bridge (LB) was investigated by Xu and Davis [1] by means of linear stability analysis (LSA) assuming the thermocapillary flow from the hot side toward the cold side near the surface and its opposing return flow near the central axis. Their result shows the neutral stability curves of $m=0$ and 1, where m denotes the azimuthal wave number. Their traveling directions of hydrothermal waves (HTWs) are opposite to (counter-flow direction) and same as (co-flow direction) the thermocapillary flow for $m=0$ and 1, respectively. Afterwards, Ryzhkov [2] revisited the LSA for the same geometry as Xu and Davis. He found a new branch of neutral stability mode of $m=1$, where HTWs are traveling in the counter-flow direction.

The experimental study in high AR (≥ 1.0) LBs of cylindrical shape is only possible under the reduced gravity condition, where AR is the relative length H/D (**Fig. 1**). Schwabe [3] studied HTWs in a LB of $AR=2.50$ under microgravity (μg) in sounding rocket. His observed HTWs are traveling in the counter-flow direction. In the recent μg experiments on the International Space Station (ISS), the traveling of HTWs in the co-flow direction are reported [4,5], where the results contrasted with the traveling direction of Schwabe. Possible reason of this contradiction is twofold: (1) large heat loss from the liquid surface in the experiment in sounding rocket and (2) considerably higher Ma than Ma_c in the experiment on ISS, where Ma is the Marangoni number and Ma_c is its critical value for the onset of instability.

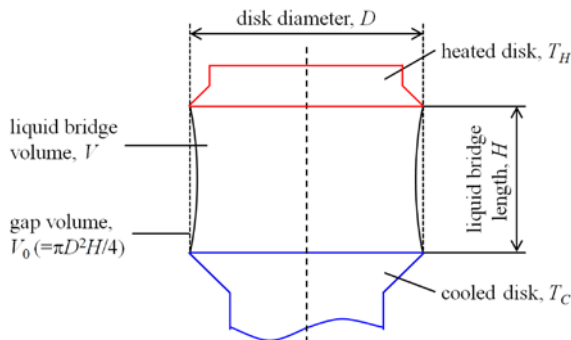The present study is focusing our interest on the instability and the flow structure of thermocapillary convection in long LBs of high Prandtl number (Pr) fluid at conditions near the onset of unsteady state, where the results were obtained under μg experiment on ISS.

2. Experiment

All the experiments have been conducted in the Fluid Physics Experiment Facility (FPEF) on ISS [4]. The geometry of our interest is a half-zone LB suspended between the cooled aluminum disk and the heated sapphire disk (**Fig. 1**). The temperature difference between those disks ΔT ($=T_H-T_C$) is the driving force of thermocapillary convection. Silicone oil with the kinematic viscosity of 5cSt ($Pr=67$) was used as the working fluid. The relative liquid volume VR ($=V/V_0$) was kept almost constant at 0.95 to prevent the liquid leakage from the edge of disks (**Fig. 1**).

Three CCD cameras observe the flow field inside the LB through the transparent sapphire disk from different viewing angles. Captured images are used to reveal the time-dependent flow structure by means of three-dimensional particle tracking velocimetry (3-D PTV). The new particle tracking algorithm is developed here and it can help us to achieve better results than the previous 3-D PTV results [5].
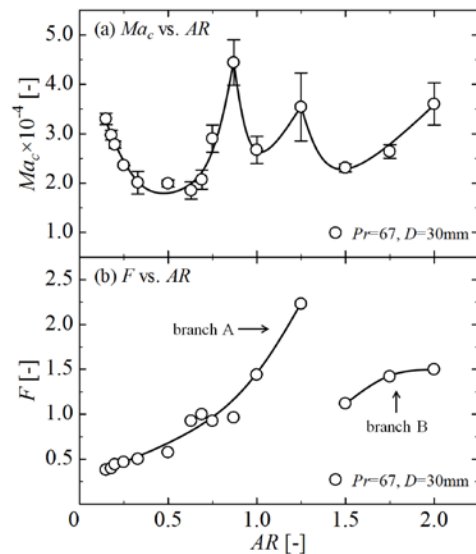

Fig. 1 Geometry of a half-zone liquid bridge

Fig. 2 Plot of Ma_c and F as a function of AR for $Pr=67$
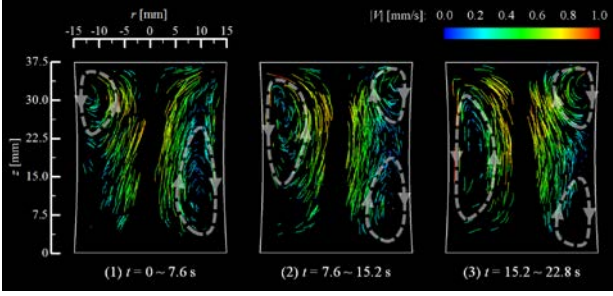
Fig. 3   Result of 3-D PTV for AR=1.25 and $Ma \approx Ma_c$.

3. Results and Discussion

Figure 2 shows the plot of (a) Ma_c and (b) dimensionless oscillation frequency F as a function of AR. Here, the respective definitions of those parameters are shown as follows:

$$Ma_c = \frac{|\sigma_T| \Delta T_c H}{\rho \bar{\nu} \alpha} \quad (1)$$

$$F = \frac{H^2}{\alpha \sqrt{Ma_c}} f \quad (2)$$

where α is the thermal diffusivity, $\bar{\nu}$ the representative value of the kinematic viscosity [4], ρ the density, σ_T the temperature coefficient of surface tension, ΔT_c the critical ΔT for the onset of unsteady flow and f the oscillation frequency. Note that the original data of Ma_c and F can be found in the literature [4]. The present Ma_c exhibits local maxima at $AR \approx 0.9$ and 1.25. At this latter AR, the present F shows a change of critical branch and it is suggesting that there is other instability mode for long LB. In this study, the branches for short liquid bridges (i.e., $AR \leq 1.25$) and long liquid bridges (i.e., $AR > 1.25$) are referred to as *branch A* and *branch B*, respectively [6].

In long liquid bridges, the surface temperature fluctuation near the critical condition is so small that the present measurement apparatuses cannot provide a sufficient temperature resolution to observe HTWs. For this reason, the instability of thermocapillary convection is approached by velocity field measured with 3-D PTV. Time series of particle trajectories on the radial/axial-plane at conditions near the onset of instability (i.e., $Ma \approx Ma_c$) for AR=1.25 and 1.50 are shown in **Figs. 3** and **4**, respectively. Note that the phase superposed particle trajectories over several oscillation periods are applied to these results. **Figure 3** shows the presence of vortical structures (VSs) near the liquid surface and they are traveling in the co-flow direction (from upper to lower). On the other hand, the traveling direction of VSs in **Fig. 4** is counter-flow direction. It is important to mention here that the corresponding F for AR=1.25 is on *branch A* and that for AR=1.50 is on *branch B*. It follows from this result that the instability mode of thermocapillary convection in long LB is changed at certain AR
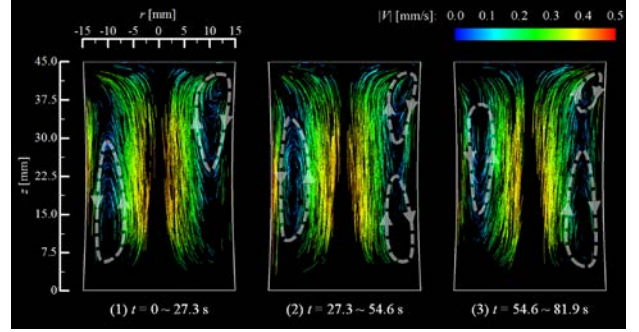

Fig. 4   Result of 3-D PTV for AR=1.50 and $Ma \approx Ma_c$.

(i.e., AR=1.25-1.50 in the present condition) and such change of the instability mode is the reason of the jump of oscillation frequency shown in **Fig. 2(b)**. As reviewed by Yano *et al*., [5, 6] the traveling of VSs is associated with HTWs, thus suggesting the possibility of the traveling of HTWs in the counter-flow direction at conditions near the *branch B*. Detailed results of the traveling of VSs and HTWs can be found in other paper written by authors. [6]

4. Conclusions

This paper reports the experimental results on the instability and associated vortical structures (VSs) of thermocapillary convection in long liquid bridges of high Prandtl number fluid (Pr=67). The flow field is measured by using three-dimensional particle tracking velocimetry (3-D PTV). The traveling of VSs is recognized after the transition to the unsteady state and its traveling directions for AR=1.25 and 1.50 are same as (from hot to cold) and opposite to (from cold to hot) the thermocapillary flow, respectively.

References

1)   J-J. Xu and S. H. Davis: Phys. Fluids, **27** (1984) 1102.

2)   I. I. Ryzhkov: Phys. Fluids, **23** (2011) 082103.

3)   D. Schwabe: Phys. Fluids, **17** (2005) 112104.

4)   H. Kawamura, K. Nishino, S. Matsumoto and I. Ueno: ASME, J. Heat Transfer, **134** (2012) 031005.

5)   T. Yano, K. Nishino, H. Kawamura, I. Ueno, S. Matsumoto, M. Ohnishi and M. Sakurai: Exp. Fluids, **53** (2012) 9.

6)   T. Yano, K. Nishino, H. Kawamura, I. Ueno and S. Matsumoto: submitted to Phys. Fluids.

環状プール内の定常表面張力対流の安定限界に及ぼす表面熱伝達の影響

○今石宣之（九州大学），M. Ermakov（Inst. Prob. Mechanics），石万元（重慶大学）

Effect of Surface Heat Transfer on the Stability Limit of Thermocapillary Flow in Annular Pool

N. IMAISHI (Kyushu Univ.), M. ERMAKOV (Inst. Prob. Mechanics), W.Y. SHI (Chongqing Univ.)

1. Introduction

Axisymmetric steady two dimensional thermocapillary flow in annular pools (depth d=1-20mm, radius of the outer wall Ro=40mm, radius of the inner wall Ri=20mm) driven by a temperature gradient in the radial direction and buoyancy becomes unstable and the hydrothermal waves[1] and other three dimensional flows set on when the temperature difference between the walls exceeds a certain threshold value. However, instability mechanism and flow modes in pools of finite extent are still not well understood. In the present work, our LSA[2] model is extended to evaluate the effects of thermal boundary conditions on the stability of buoyant-thermocapillary flow in annular pool.

2. LSA Model

LSA model assumes a thin solid layer (thickness d_b and thermal conductivity k_b) between the pool bottom and a base plate which has a steady conductive temperature distribution in the radial direction. Thermal conductance between the base plate and the liquid pool is expressed by the Biot number $Bi_b=k_bd/k_ld_b$. In this work, we assume $Bi_b=0$, i.e., the pool bottom is adiabatic. $Bi_T=hd/k_l$ is used for the thermal conductance between the liquid surface and the ambient gas at a uniform temperature T_a. The details and calculation method were described at JASMAC-27.

3. Result and discussion

3.1 Effect of Θ_A and Bi_t on 3-D flows of medium Pr fluid.

As was reported at the JASMAC-27, small heat loss from the liquid surface reduces $Re_c = \sigma_T \Delta T_c (R_o - R_i)/\mu\nu$ for HTW1 but larger heat loss increases Re_c significantly for a shallow pool of medium Pr fluid (Pr=6.7, d=1.0mm, $Bi_b=0$, 0G). On the other hand, heat gain from the gas phase always stabilizes the steady axisymmetric flow against HTW1. It should be noted that Bi_T and $\Theta_A=(T_a-T_c)/(T_h-T_c)$ lead to the adverse effects on HTW2. The effect of Bi_t and Θ_A on stability limits are shown in Fig.1 and Fig.2 for shallow (d=1.0mm) and medium (d=5mm) pools, respectively. The critical Reynolds number (Re_c) and critical temperature difference (ΔT_c) depends on pool depth and Θ_A as shown in Fig. 3 for Pr=6.7 under 0G. These results show the significant effects of the surface heat transfer on ΔT_c as well as
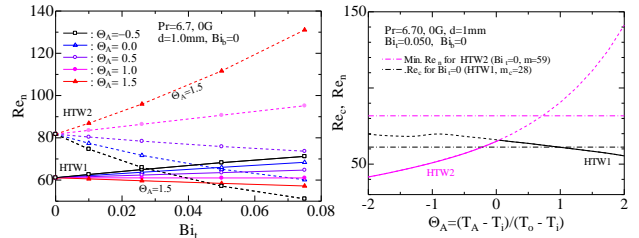

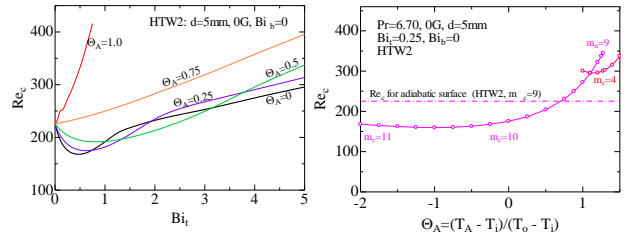Fig. 1 Effects of Bi_T and Θ_A on the neutral condition (d=1mm).

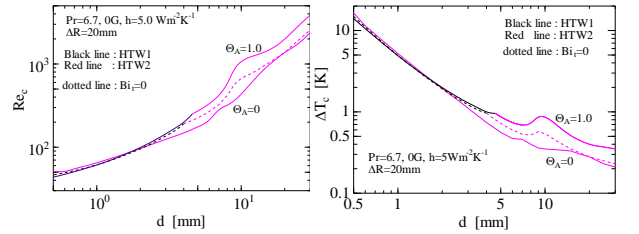Fig. 2 Effects of Bi_T and Θ_A on the neutral condition (d=5mm).

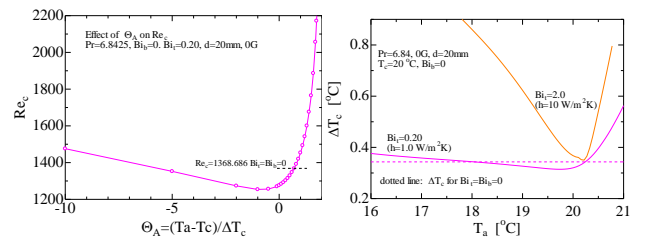Fig. 3 Re_c and ΔT_c as a function of d and Θ_A (Pr=6.7, 0G).

Fig. 4 Effects of Θ_A on the critical conditions (Pr=6.84, d=20mm).

the azimuthal wave number m_c and oscillation frequency f_c.

In shallow pools, HTW2 becomes the most dangerous mode under large heat loss. In deeper pools, HTW2 is the most dangerous mode and large heat gain tends to increase ΔT_c and reduce the wave number. Reduction of m_c by heat gain becomes most significant in pools with medium depth. LSA results for Pr=6.84 predicts that Re_c (ΔT_c) values are about twice of those reported by Sim et al[3]. Fig.4-b suggests that the ambient

temperature T_a and heat transfer coefficient h causes significant change of ΔT_c, especially when T_a is higher than the outer wall. However, high heating destabilizes the basic flow at Re>3400. Thus LSA can't provide quantitative explanation for the space experiment results of MAGIA[3] ($Re_c \approx 7000$ for d=20 mm).

In case of buoyant-thermocapillary flow under 1G condition, the stability diagram becomes more complex because a flow mode change from HTW1 to HTW2 occurs at small depth and 3D steady flow occurs in deeper pools. For a case of d=1mm, the stability diagram seems similar to that shown in Fig.1. Effect of Bi_t and Θ_A on the stability of a pool of d=5mm shown in Fig.5 indicates that 3DSF is the most dangerous mode for adiabatic pool, heat gain and small heat loss cases. However, under large surface heat loss the basic flow becomes unstable at smaller Re value against HTW2 .

Fig.5 Effects of Bit and Θ_A on the critical conditions in an annular pool against of d=5mm, Pr=6.7 under 1G.

3.2 Effect of Θ_A and Bi_t on 3-D flows of a low Pr fluid.

In shallow pools of low Pr fluids, the Marangoni effect driven by the radial temperature gradient induces a strong basic flow and this basic flow becomes unstable against 3D perturbations and 3-D oscillatory flows OSC1 or OSC2 and 3D steady flow 3DSF1 set on at a certain threshold Reynolds number.

Fig.6 shows the neutral stability curves for each flow mode as a function of Bit for Pr=0.011, d=1.0mm under 1G and Θ_A=0. It should be noted that this figure covers a very wide range of h values since Bi_t=0.001 corresponds to h=64 W/m²K.

In the basic flow placed in an environment of Θ_A=0, radial temperature gradient near the outer pool increases at Bi_t>0.001, and the most dangerous 3-D flow mode changes from OSC1 to OSC2. When Bi_t exceeds 0.00488 at 1G a 3D steady flow (3DSF3) becomes the most dangerous mode and a flow mode
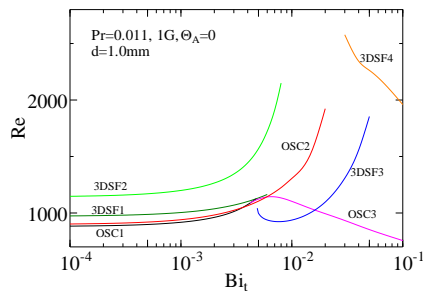

Fig.6 Effect of Bit on the neutral stability curves for Pr=0.011 d=1.0mm,

(OSC3) appears at Bi_t>0.016.

Effects of Θ_A on the neutral stability conditions for d=1mm, 1G, Bi_b=0 and Bi_t=0.003 (h=192W/m²K) is shown in Fig.7. Appearance of 3DSF3 and OSC3 correspond to the large deformation of the basic flow field from that in the pool with an adiabatic surface (Bi_t=0) caused by interfacial heat transfer.
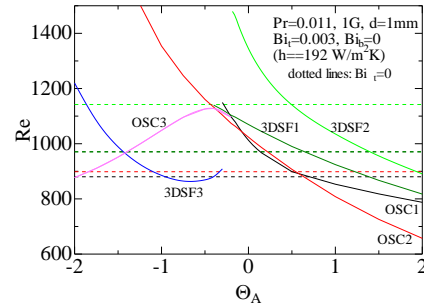

Fig.7 Effect of Θ_A on the neutral stability curves.

In case of deeper pools, the neutral stability branches of 3DSF locate far above that of oscillatory flow modes and the effects of the surface heat transfer is less significant than for shallow pools.

4. Conclusion

Linear stability analyses foe annular pools revealed the detailed effects of the thermal boundary condition on the pool surface for medium and low Pr fluids as follows.

1) In case of medium Pr fluids, surface heat loss stabilizes the basic flow against HTW1 but destabilizes against HTW2. Heat gain from the ambient gas phase works in the opposite way. These effects cause disappearance of HTW1 in shallow pools under large heat loss conditions.

2) In case of medium and large depth pools of medium Pr fluids, small heat loss destabilizes against HTW2 but larger heat loss stabilizes and increases m_c. Heat gain largely stabilizes the basic flow and reduces m_c.

3) Large heat loss from the surface gives small effects on the 3DSF in medium Pr pool, on the other hand, destabilizes against HTW2. Therefore, large heat loss causes change of critical flow mode from 3DSF to HTW2 in pools of medium depth under 1G .

4). Neutral stability curves for low Pr liquid's pool show strong and complex Bi_t and Θ_A dependencies. Under large surface heat fluxes, new flow modes, such as 3DSF2 and OSC3, set on. These flow modes correspond to big change of the basic flow field caused by the surface heat flux.

References
1) M.K. Smith and S.H. Davis: J. Fluid Mech., **132** (1983) 119.
2) WY Shi, M. Ermakov and N. Imaishi: J. Crystal Growth, **294** (2006) 474.
3) B.C. Sim, A. Zebib and D. Schwabe, J. Fluid Mech., **491**(2003) 259.

容器内動的濡れ挙動のＣＦＤ解析

○今井良二（室工大）

CFD Analysis for Dynamic Wetting Behavior in a Container

○Ryoji IMAI (Muroran Institute of Technology)

1. Introduction

Fluid behavior in microgravity (μg) is different from in ground gravity since surface tension, viscous force, and wetting are dominant in μg condition. In propellant tank for artificial satellite and future on-orbit spacecraft, sloshing due to disturbance and settling behavior by change of acceleration have to be understood for design of propellant supply system and attitude control system.

In past years, many researches for fluid behavior in tank have been done, however, in general, dynamic contact angle and dynamic wetting; main parameters which characterize μg fluid behaviors, have been treated empirically. On the other hand, there are large number of researches for dynamic wetting in ground gravity [1]. However, dynamic wetting phenomena have not been fully understood since there are difficulties in treating from micro to macroscopic physics. In addition of this, these studies targeted small scale objects such as capillary tube and droplet, therefore there are less studies treating relation between dynamic wetting and macroscopic fluid behavior under μg condition in which dynamic wetting is dominant even in large scale object.

Our final target is to understand how dynamic wetting affect macroscopic and large scale fluid behavior in μg condition. This paper describes results of CFD analyses which investigate the effect of theoretical and empirical equations for dynamic contact angle on fluid behaviors in μg condition.

2. Numerical calculation of fluid behaviors in cylindrical container considering dynamic wetting

Fluid behaviors without gravitational force driven by dynamic wetting in cylindrical container were analyzed by commercial CFD code ANSYS FLUENT. VOF (Volume of Fluid) method was employed to calculate two phase flow, and geometric reconstruction scheme was applied as an interface reconstruction algorithm. Surface tension was considered in momentum equations by CSF (Continuum Surface Force) method. Dynamic contact angle was applied as a boundary condition on cylindrical wall. There are many equations for dynamic contact angle which has dependency of contact line velocity by theoretical and empirical approach. Cox's [2] and Kato's [3] formulae were used to provide dynamic contact angle, and values of empirical coefficients in these formulae were assumed to be same as ones used in Kato's paper [4]. Contact line velocity was obtained by multiplying velocity vector on numerical cell neighbored on sidewall and unit gradient vector of VOF.

Table 1 shows fluids and these properties. Static contact angle was assumed to be 0 degree. In this calculation, diameter and height of cylindrical container was 0.01m and 0.03m respectively.

Figure1 shows snapshot of liquid behavior, that is volume ratio of liquid. It is found that liquid behavior depends on formula for dynamic contact angle; rising speed along side wall is largest in Cox's formula, and in Kato's formula, thin liquid film was not formed on the upper area of side wall.

Table 1 Thermal properties

Liquid phase	Silicon oil
Density	818 kg/m^3
Viscosity	8.18x10^{-4} Pas
Gas phase	Air
Density	1.225 kg/m^3
Viscosity	1.7895x10^{-4} Pas

3. Conclusion

Numerical calculation was made to investigate the influences of theoretical and empirical formulae of dynamic contact angle on fluid behaviors in cylindrical container. As a next step, we will conduct short term microgravity experiment and construct a theoretical model to realize effect of dynamic wetting phenomena on macroscopic fluid behavior in μg condition.

References

1) T. D. Blake,: J. of Colloid and Interface Science, **299**(2006) 1.

2) R. Cox: J. of Fluid Mechanics, **168**(1986) 169.

3) K. Kato, T. Wakimoto, S. Nitta: J. Jap. Soc. Exp. Mech. **10**(2010) s62.

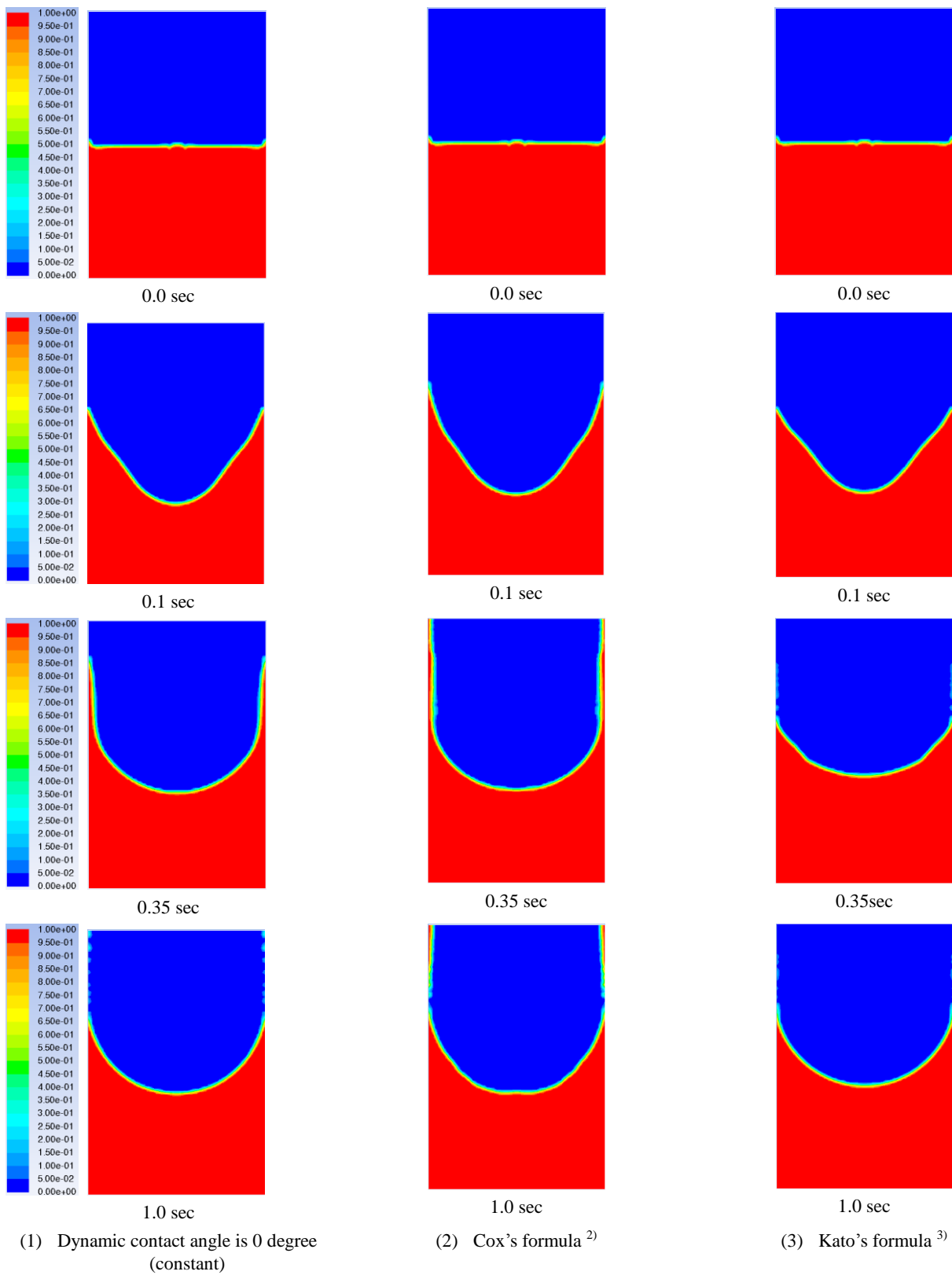4) K. Kato, T. Wakimoto, Y. Yamamoto, T. Ito: Experimental Thermal and Fluid Science Available online (2014).

0.0 sec   0.0 sec   0.0 sec

0.1 sec   0.1 sec   0.1 sec

0.35 sec   0.35 sec   0.35sec

1.0 sec   1.0 sec   1.0 sec

(1) Dynamic contact angle is 0 degree (constant)   (2) Cox's formula [2]   (3) Kato's formula [3]

Fig.1 Snap shot of liquid behavior

(Contour of volume fraction of liquid)

月レゴリスシミュラントの溶融塩化学

○後藤琢也，坂中佳秀（同志社大学），福中康博（早稲田大），
M.V.クマール，石川毅彦 （JAXA）

Utilization of Lunar Resource by using Molten Fluoride Technology

Takuya GOTO, Yoshihide SAKANAKA (Doshisha Univ.), Yasuhiro FUKUNAKA(Waseda Univ.),
M.V. KUMAR, Masahiro TAKAYANAGI(JAXA)

1. Introduction

In-situ resource utilization for space activity is very important for realizing the construction of lunar base. Electrochemical extraction of silicon from regolith is an attractive method from the point of view of space utilization, because the method gives not only silicon for solar cell but also oxygen for human activity. Development of a new oxygen evolution electrode in molten fluorides is thus required, since molten fluorides are expected to be an electrolyte for electrochemical reduction process of lunar regolith. An inert electrode available for oxygen evolution in molten fluorides at elevating temperatures has thus been investigated by many researchers. Considering sustainability of the processes, the anode composing of nontoxic and abundant materials is preferential. In this study, $FeAl_2O_4$, hercynite has been selected and attempted to be prepared by a conventional ceramic method. Structure, morphology and resistivity of the obtained sample at room temperature were studied. Oxygen evolution behavior was also investigated in a LiF-KF-NaF melt to test the possibility of a new anode.

2. Experimental

The regent grade raw materials of γ-Al_2O_3 and α-Fe_2O_3 in molar ratio of 2.0 were mixed with alcohol and calcined at 1123 K under a N_2–10vol% H_2 flow for 2 h to form $FeAl_2O_4$ powder. The obtained sample was compacted by CIP of 200 MPa to obtain a square-pole shape. The compact was then sintered at 1723 K for 8h in a N_2 - 0.1 vol% H_2 gas flow. The samples were characterized by an x-ray diffraction. A scanning electron spectroscopy and four contact conductivity measurement was carried out at room temperature. Electrochemical measurement in a LiF-NaF-KF eutectic was carried out by a three electrode system under argon atmosphere. Lithium oxide (Li_2O) was used as the oxide ion source. The working electrode was a hercynite electrode and the counter electrode was a glassy carbon rod. The reference electrode was an Ag^+/Ag electrode and the potential of this reference electrode was calibrated with reference to deposition potential of potassium[1].

3. Results and discussion

The X-ray diffraction patterns of calcinated powder and sintered hercynite ceramics are shown in Fig. 1. Fig. 1(a) is the XRD patterns of hercynite powder calcinated at 1173K for 6h in the N_2 - 1 vol% H_2 atmosphere, and (b) is the XRD patterns of hercynite ceramics sintered at 1623K for 6h N_2 – 0.1 vol% H_2 atmosphere. Each observed peaks were identified as $FeAl_2O_4$. And the relative density of obtained hercyite ceramics was 99.8% measured by Archimedes'method.

The electrode behaviors of oxide ions in a LiF-KF-NaF melt with $FeAl_2O_4$ and SiC electrodes were investigated by cyclic voltammetry. On the anodic sweep, anodic current was observed with shown as following reaction.

$$O^{2-} \rightarrow 1/2O_2 + 2e^-$$

In order to test the stability of $FeAl_2O_4$ and SiC electrodes, galvanostatics electrolysis at 50mA was carried out for 1h in a molten LiF-NaF-KF containing SiO_2 at 773K. The result is shown in Fig.2 and the availability as inert anode of $FeAl_2O_4$ and SiC electrodes was confirmed, because steady current and steady potential were observed during electrolysis in both cases.
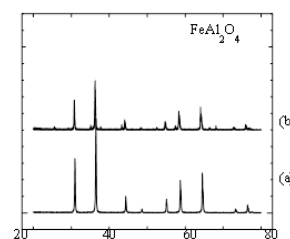

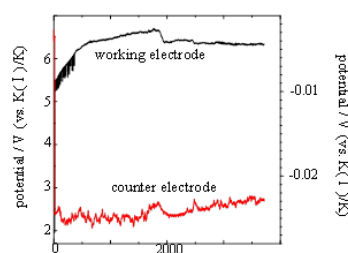Fig 1. XRD pattern of $FeAl_2O_4$: (a) calcinated powder; (b) hercynite ceramic.

Fig 2. Potential of working electrode ($FeAl_2O_4$) and counter electrode (Al plate) during galvanostatics electrolysis.

電磁浮遊融液からの一方向凝固による Fe リッチβ-FeSi₂ の組織と熱電特性

○永井秀明（産総研），山田高広（東北大）

Thermoelectric Properties and Morphology of Fe-rich β-FeSi₂ Prepared by Unidirectional Solidification from Electromagnetic Levitated melts

○Hideaki NAGAI (AIST), Takahiro YAMADA (Tohoku Univ.)

1. Introduction

β-FeSi₂ is known as one of the high temperature thermoelectric materials. This material consists of Fe and Si, and both elements exist enough in the earth. However, single phase β-FeSi₂ bulk sample shows low thermoelectric performance because of high thermal conductivity and insufficient electric conductivity. Our previous work has revealed that β-FeSi₂ sample with aligned FeSi phase improved the thermoelectric performance[1]. In this way, the modification of morphology of β-FeSi₂ sample, such as introduction of second layer with electrical conductive nature (FeSi) and the micropores etc., is one of the possibilities to improve the thermoelectric performance. In this study, we synthesized Fe-rich β-FeSi₂ by solidification from electromagnetic levitated (EML) melts and the following annealing to control the morphology of the sample and evaluated the thermoelectric properties.

2. Experimental

Starting Fe-Si compounds were prepared by arc-melting of the constituent elements ([Fe+Co]:Si=35.3:64.7, Fe:Co=95:5 [in mole]). The arc-melted sample was cut into the suitable size. This sample block was set on the unidirectional solidification system using electromagnetic levitator, as shown in Fig.1. In this system, the levitated sample was cooled by helium gas flow (1L/min) and dropped on the cooling chill (BN, Si, Cu blocks, and Cu block with Sn layer). Sample temperature was measured by optical pyrometer from the upper sides of the system. The obtained samples were analyzed by XRD, SEM before and after annealing at 1073 K for
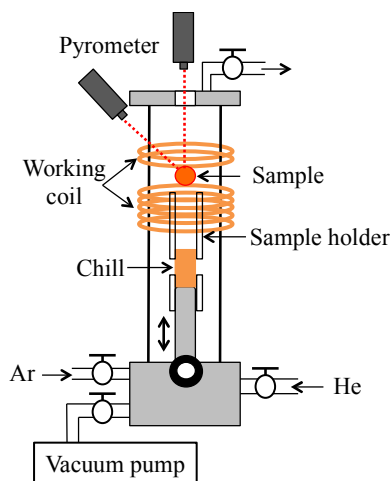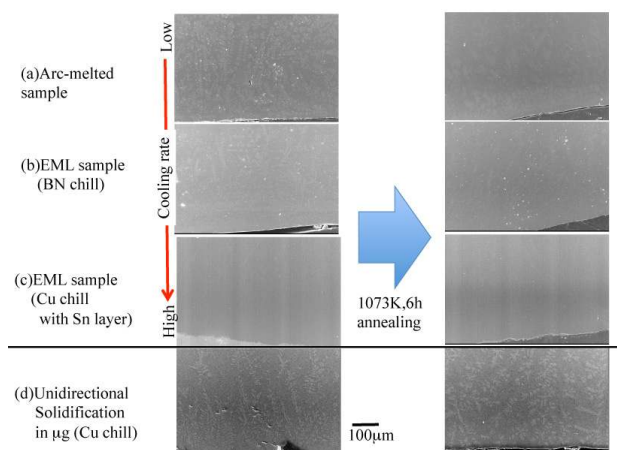

Fig.1 Unidirectional solidification system by electromagnetic levitator

6h. The thermoelectric properties were evaluated by electrical conductivity and Seebeck coefficient after annealing.

3. Results and Discussion

All solidified sample were mixture of α-FeSi₂ phase and FeSi phase. Arc-melted sample had coarse FeSi phase with some alignment along cooling direction because of low cooling rate. The microstructure of EML samples became fine, as shown in Fig.2, because of higher cooling rate than that of arc-melted sample, but the samples had less orientation of FeSi phase. The samples solidified with BN and Cu cooling chill, and Si chill from different melt temperature had similar microstructures. Because the wettability between sample melt and cooling chill was bad, the cooling rates of the melts were considered to be similar. Our previous work reported that high cooling rate was achieved by splat-solidification of FeSi₂ melt on Cu chill block with Sn layer[2], because of good contact between FeSi₂ melt and cooling chill. When Cu block with Sn layer was used as cooling chill, the sample melt had good contact with cooling chill and higher cooling rate was obtained. Due to the higher cooling rate, the sample had quite fine microstructure without dendrite structure. This area thickness was about 200μm. Some FeSi phase dendrite structure without orientation appeared above the area, and the microstructure far from the cooling chill was similar to those solidified by other cooling chill because of decreasing the cooling rate. On the other hand, the microstructure synthesized by unidirectional solidification in μg had rather coarse FeSi phase with alignment along cooling direction. After annealing, the area of FeSi phase decreased

Fig.2 Microstructures of Fe-rich FeSi₂ alloys solidified from melts and their annealed samples.

and network of FeSi phase became poor. This tendency was remarkable as microstructure of FeSi phase became fine, and the FeSi phase in the EML samples was mostly dispersed in the matrix without orientation. Both arc-melted sample and EML samples rarely had the mixture area of β-FeSi$_2$ phase and Si phase, which was created by decomposition of α-FeSi$_2$.

Figure 3 shows the thermoelectric properties of Fe-rich β-FeSi$_2$ with different microstructure after annealing. EML samples had lower conductivities than that of arc-melted sample because of fine microstructure. On the other hand, the conductivity of the sample synthesized by unidirectional solidification in μg increased with temperature, and higher conductivity was achieved at high temperature. Seebeck coefficient of EML sample using Cu block with Sn layer was lower than those of other samples. Because this sample still remained fine microstructure after annealing, insufficient crystal growth of β-FeSi$_2$ phase was considered to decrease the value of Seebeck coefficient. As a result, the thermoelectric performance of the sample with fine microstructure and poor network of FeSi phase without orientation was lower than those of other sample.

Fig.3 Thermoelectric properties of Fe-rich β-FeSi$_2$ with different microstructure

References

1) H.Nagai, D.Saito and T. Okutani: Abst. of 27th Jpn. Soc. Microgravity Appl. Conf., Nov., 2013, 92.

2) H.Nagai, Y.Nakata, M.Shibuya and T.Okutani: Jpn. J. Appl. Phys., **42** (2003) 1690.

<div align="center">

JEM 与圧部および曝露部における微小重力環境

</div>

○石川巨樹（株式会社エイ・イー・エス），伊藤剛，小仁所裕喜子（宇宙航空研究開発機構）

<div align="center">

Microgravity Environment of JEM Pressurized Module and JEM Exposed Facility

</div>

○Naoki ISHIKAWA (Advanced Engineering Services, Co., Ltd)

Tsuyoshi ITO, Yukiko KONISHIO (Japan Aerospace Exploration Agency)

1. Introduction

Microgravity environment is one of the most favorable characteristics for science experiment in the Japanese Experiment Module (JEM). However, it is disturbed due to vibration caused by movement of crew members, onboard equipment operations and docking event of visiting vehicle, etc. JAXA has measured the disturbance in JEM Pressurized Module (JPM) using Microgravity Measurement Apparatus (MMA) since 2008 and that on JEM Exposed Facility (JEF) using Microgravity Measurement Equipment (MME) since 2013 because those data are necessary for planning experiment utilizing microgravity condition.

The disturbance data acquired by the MMA has been already analyzed and reported.[1, 2] Furthermore, additional data recently taken by the MME could provide more detailed microgravity environment data to experiment users in the JEM.

2. Accelerometer Description

2.1 Microgravity Measurement Apparatus (MMA)

Three MMAs are located in experiment racks in the JPM and each MMA has acceleration sensors in three directions as shown in **Fig. 1** and **Table 1**. The maximum sampling frequency is 1220Hz and the maximum cutoff frequency is 300Hz.
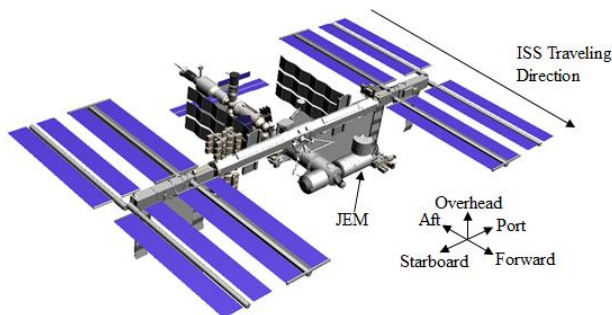

Fig. 1 ISS and JEM Direction

Table 1 MMA Sensors Direction and Locations

Location	Direction		
	+X	+Y	+Z
Saibo Rack	Overhead	Starboard	Forward
Ryutai Rack	Overhead	Starboard	Forward
Kobairo Rack	Overhead	Port	Aft

2.2 Microgravity Measurement Equipment (MME)

There are three MMEs on the JEF with three measurement mode (**Table 2**). Each MME has acceleration sensors in three directions as shown in **Fig. 2**.

Table 2 MME Specification

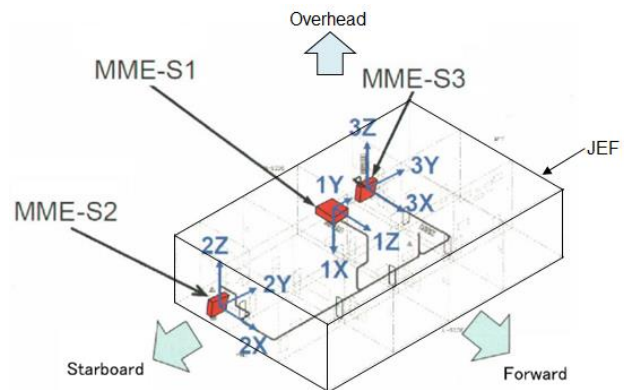| Measurement mode	Frequency range [Hz]	Sampling frequency [Hz]	Acceleration range [G]
Low	0.01~10	100	$5 \times 10^{-7} \sim 2 \times 10^{-3}$
High	5.0~300	2000	$5 \times 10^{-6} \sim 2 \times 10^{-2}$
Extension	5.0~300	2000	$5 \times 10^{-5} \sim 2 \times 10^{-1}$

Fig. 2 MME Sensors Location and Direction

3. Analysis Result

One-third octave band analysis results and spectrogram of measurement data acquired by MMA on Ryutai Rack and MME-S2 are shown in **Fig. 3** thru **Fig. 7**. Those data had been acquired for 15 hours (GMT18:00 - 09:00) without special g-jitter event, such as docking of visiting vehicle. This time, sampling frequency and cutoff frequency of the MMA was 1220Hz and 300Hz. The MME had taken the data in low mode.

For forward direction and overhead direction, the MME shows higher acceleration at around 0.2~0.9Hz compared to the MMA, though no major difference is found for starboard direction.

It is known that the ISS has a natural frequency at around

0.25~0.3Hz. It is considered that JEF is more affected be natural vibration of the ISS than JPM because the JEF is attached at port side of the JPM which is more distant from gravity center of the ISS. Therefore, it is presumed that the acceleration data taken by the MME is affected by the natural frequency of the ISS.
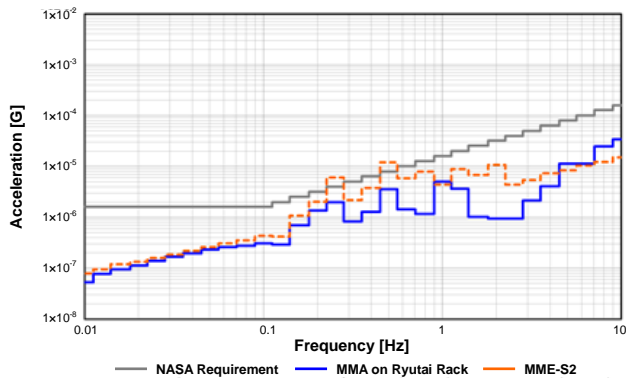

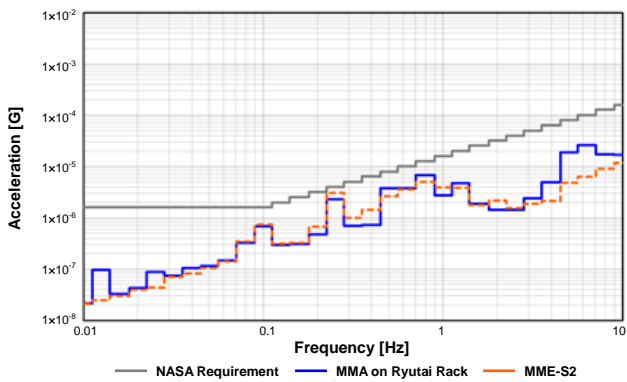**Fig. 3**　One-third Octave band (ISS forward direction)

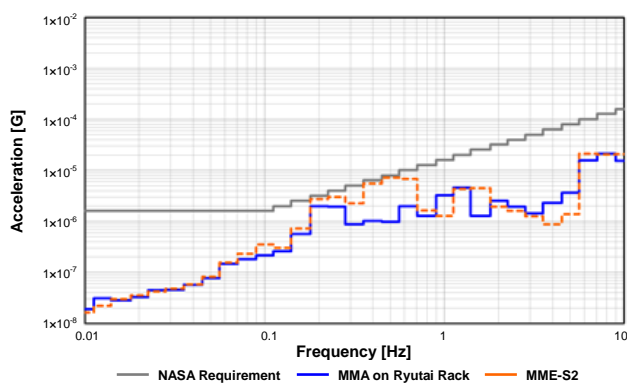**Fig. 4**　One-third octave band (ISS starboard direction)
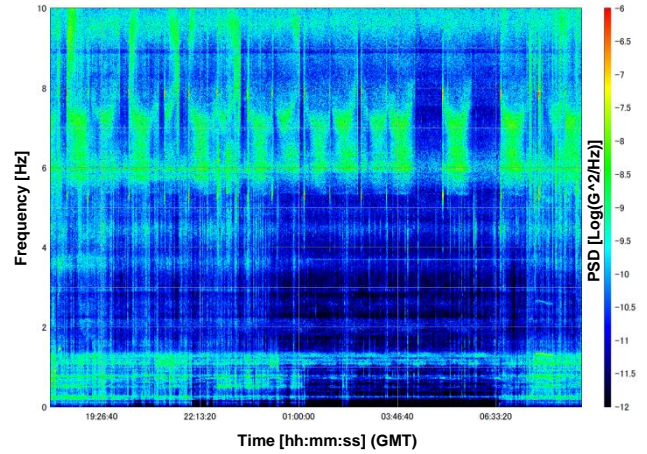

Fig. 5　One-third octave band (ISS overhead direction)

Fig. 6　Spectrogram (MMA on Ryutai Rack)

Fig. 7　Spectrogram (MME-S2)

4. Conclusion

Microgravity environment data taken by both MMAs and MMEs for 15 hours a day without special g-jitter event has been analyzed. The results show that the environment on the JEF is affected by the natural frequency of the ISS, and it is different from that in the JPM. In addition, it was found that the MMA on Ryutai Rack and MME-S2 is respectively sensitive to the vibration at different frequency due to the structural characteristics.

Studying microgravity environment in both the JPM and the JEF is effective method to comprehensively understand JEM microgravity environment. We will continue analyzing the JEM microgravity environment with this method in order to achieve good experiment results in low-disturbance microgravity environment.

References

1)　M. Goto, K. Murakami, H. Ohkuma: J. Jpn. Soc. Microgravity Appl, **Vol.28 No.1** (2011) 8

2)　H. Ohkuma, K. Murakami, M. Goto: J. Jpn. Soc. Microgravity Appl, **Vol.28 No.1** (2011) 13

JEM 搭載微粒化観察装置の開発状況その２

○大熊隼人，中村裕広，菊池政雄，伊藤裕一，柚木園諭（JAXA），梅村章（名産研），中神秀俊，
瀬良暁雄，古友大輔，小林涼華（千代田化工建設）

The Status of Development of Atomization Observation Equipment in JEM 2

○Hayato OHKUMA, Yasuhiro NAKAMURA, Masao KIKUCHI, Yuichi ITO, Satoshi YUKIZONO (JAXA),
Akira UMEMURA (NISRI) , Hidetoshi NAKAGAMI, Akio SERA, Daisuke FURUTOMO, Ryoka KOBAYASHI
(Chiyoda Co., Ltd)

1. Introduction

Liquid atomization is a very important to spray combustion. However, atomization mechanism is poorly understood due to the technical diffculty that the phenomenon ends with an extremely short period and tiny scale that it only can be interpreted by high-speed camera technique. JAXA has newly developed Atomization Observation Equipment (hereafter refered as AOE) for space experiment in Kibo/ISS. The purpose of this experiment is validation of the new atomization concept by observing the breakup behaviors of water jets in closeup. At this experiment, water is injected from syringe. Then the water is atomized after a period of time. We shoot the behavior with high-speed camera.

AOE will be attached to the Work Volume (hereafter refered as WV) section of the Multi-purpose Small Payload Rack (hereafter refered as MSPR) in Kibo.

2. Space experiment in JEM

We will observe the breakup behaviors of water jets under control of water injection speed. The speed is changed in following three type.

The vertical axis in each graph is injection speed. And horizontal axis is time.

On Type A, injection speed is continuously changed in order to investigate atomization hysteresis. Type B is intermittent injection type. We will compare the result of experiment Type A and Type B. The water is injected at a constant rate on Type C. We expect to acquire correlation function of breakup distance in this type.

3. Overview of Equipment

AOE has mainly three functions. First function is speed control of injection water. The second is acquiring the image of water jet with high speed camera. The last function is measurement of various data such as water speed and temperature.
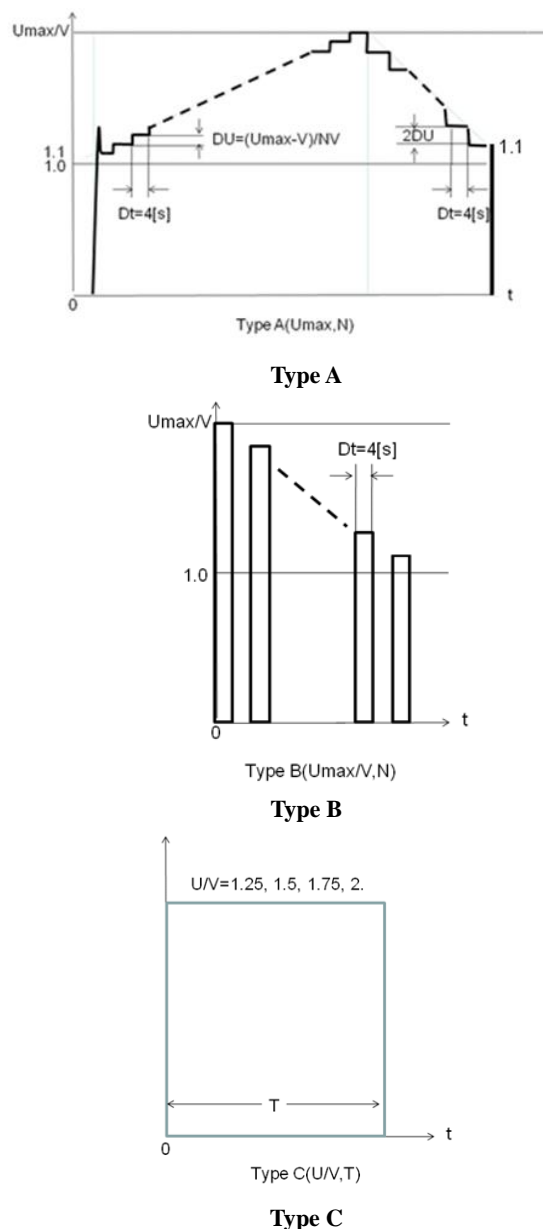

Type A

Type B

Type C

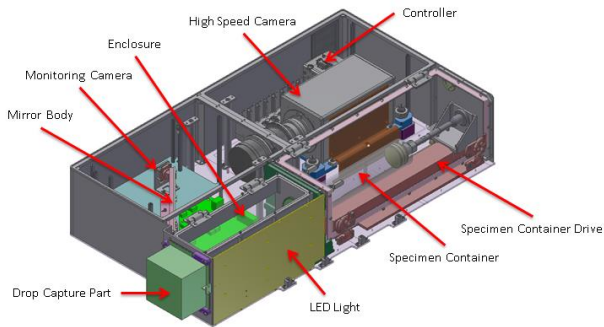**Fig. 1**　Injection Speed Type

Fig. 2 Atomization Observation Equipment

The function and specification of each component are as follows.

[Enclosure]

Enclosure is a container in which water is injected. Side wall has a transparent window for observation with high-speed camera. Enclosure is made of aluminum alloy plate and the window is made of Polycarbonate.

[Specimen Container Drive]

Specimen Container Drive is a linear drive porter with linear encoder, to drive the Specimen Container at the designated speed. The travel of the drive is about 260mm. Linear encoder has an optical marker to precisely measure and control the position of the drive.

[High Speed Camera]

High Speed Camera equipped with an electric zooming/focusing lens is to capture the high speed image of water injection. All operations are executed automatically including the focusing and zooming which is performed from the ground by telecommandings.

[Monitoring Camera]

Monitoring Camera is a CCD Camera which acquires the general image of the experiment.

[LED Light]

LED Light is an array of white LED chips. It is to illuminate the water jet for image acquisition with High Speed Camera.

[Specimen Container]

Specimen Container is a cylindrical chamber made of plastic that store water inside. 400ml of water is stored in one container.

[Drop Capture Part]

Drop Capture Part catches injected water. Inside of the part is conically shaped and lined with sponge-like absorbent. One Drop Capture Part can hold up to 700ml of water capability.

4. Status of development

We have fabricated AOE's Prototype Flight Model（PFM）and finished the Proto Flight Test (PFT).

Currently we are acquiring ground experiment data. We will report the result of ground experiment in the presentation

References

1) A. Umemura, S. Kawanabe, S. Suzuki & J. Osaka, Phys. Rev. E, 84(2010) 036309.

2) A. Umemura, Phys. Rev. E, 83(2011) 046307.

液滴群燃焼実験供試体フライトモデルの開発状況

○菅 勇志，菊池 政雄，高柳 昌弘，水島 隆成（JAXA）

Dvelopment status of Group Combustion Experiment Module Flight Model

Yuji KAN, Masao KIKUCHI, Masahiro TAKAYANAGI, Takanari MIZUSHIMA (JAXA)

1. Outline

Elucidation of Flame Spread and Group Combustion Excitation Mechanism of Randomly-distributed Droplet Clouds is the objective of the "Group Combustion", to be performed as a Japanese Experiment Module/KIBO second phase utilization. "Group combustion" experiment is planned to employ the Multi-purpose Small Payload Rack (MSPR) and the Chamber for Combustion Experiment (CCE) which were installed in KIBO. We report the development status of GCEM Proto Flight Model(PFM)

2. Outline of the Experiment Module

Combustion Experiment Module is installed inside the Chamber for Combustion Experiment (CCE) which is installed in Multipurpose Small Payload Rack(MSPR). CCE is one of the components of the MSPR(see Fig. 1).
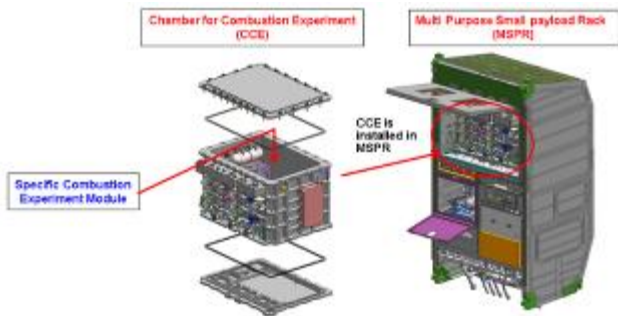

Fig. 1 Overview of the experiment MSPR/CCE

Group Combustion Experiment Module (GCEM) is composed of Small Combustion Vessel, Fuel Supply Unit, Observation Unit, Communication Control Unit, Gas Supply/Vent Plumbing Unit, Gas bottle A Assy, and Filter(see Fig. 2).
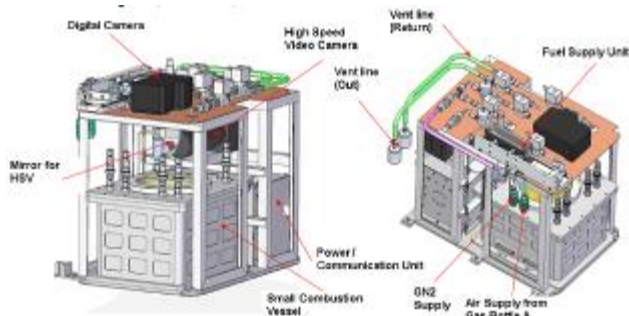

Fig. 2 Overview of the GCEM

3. Development Status

3.1. Current Status

Production of GCEM PFM has been completed(see Fig 3, Fig 4, Fig 5). GCEM PFM passed Function Test, Vibration Test, EMC Test, Fit Test, and more some Tests.

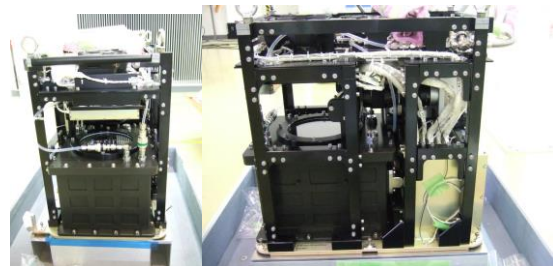Group Combustion passed PSRP Phase 0/1/2/3 on last June and passed the PQR last July.
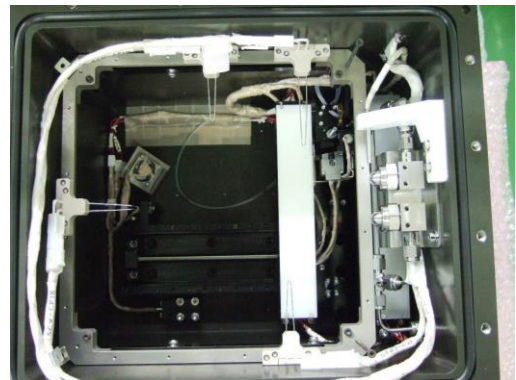

Fig. 3 GCEM FM

Fig. 4 Combustion Vessel

Fig. 5 Gas Bottle A ASSY

4. Schedule

GCEM PFM will launch by Orb-4 in April 2015. The experiment on orbit will start after launch.

Before launch, Gas Bottle A ASSY will be filled Gas(O2+N2) at the Wallops Flight Facility.

酸素製造装置の軌道上実証

○桜井 誠人，島 明日香，大西 充（JAXA）

ISS Demonstration of Oxygen Generation

○Masato SAKURAI, Asuka SHIMA, Mitsuru OHNISHI (JAXA)

1. Introduction

In order to reduce the amount of water that must be carried on future space mission closed-cycle air regeneration system is being developed[1]. In such a system, CO_2 exhaled by astronauts as a product of respiration is continuously removed from the spacecraft's atmosphere and combined with H_2 to produce water by the Sabatier reaction. The process is exhaled carbon dioxide is concentrated in an absorbent using a pressure and temperature swing, then reduced by the Sabatier reaction $(CO_2 + 4H_2 \rightarrow CH_4 + 2H_2O)$ to produce water and methane. The water is then electrolyzed to produce oxygen which is consumed again by the crew.

2. Water Electrolysis

It is necessary to produce dry oxygen for human breathing, One way to produce dry oxygen from water electrolysis is by supplying water only to the cathode or hydrogen-generating side of the cell as shown in Fig. 1, since electro-osmosis produces a force to expel water from the cathode.

Two water electrolysis cell stacks were prepared by Daiki Ataka Engineering Co. Ltd. One was a conventional design 10-cell stack using a Nafion 114 proton exchange membrane, each cell having a catalyst surface area of 64 cm^2. The other was a controlled cathode feed design comprising of a 3-cell stack with an improved electrolyte, each cell having 64 cm^2 of catalyst area. The operating characteristics of the conventional and controlled cathode feed designs are shown in Fig. 2. The stacks were operated at 30°C with a controlled back pressure of 0.1 MPa. With increasing current density, the cell voltage of the conventional design stack rose rapidly, while that of the controlled cathode feed design remained relatively flat.

3. A membrane type water/gas separator

A technical issue with space electrolysis systems is that gas-liquid separation is fundamentally different in a microgravity environment to its behavior in a gravity field. A membrane type water/gas separator consisting of hydrophilic and hydrophobic membranes was used. The membrane is visible through the transparent cover of the separator.

When the gas/liquid separator is installed vertically, bubbles collect in its upper side, while bubbles spread throughout the separator when it is installed horizontally. The pressure drop of the membrane type water/gas separator is shown in Fig. 3.

References

1) M. Sakurai, et.al. "Development of Oxygen Generation Demonstration on JEM (KIBO) for Manned Space Exploration" Proc. ICES-2014-125 (2014)
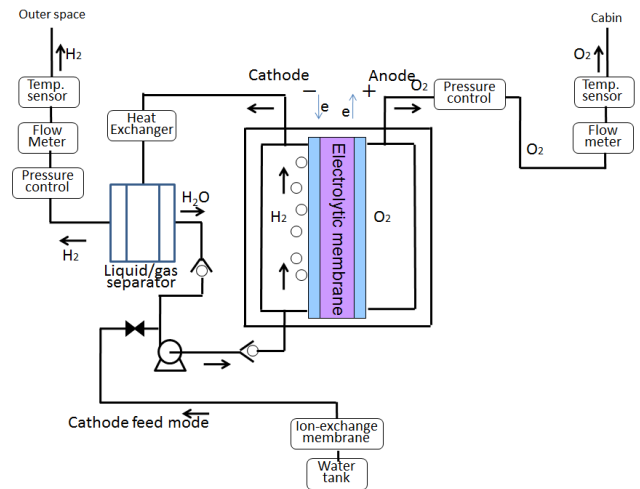
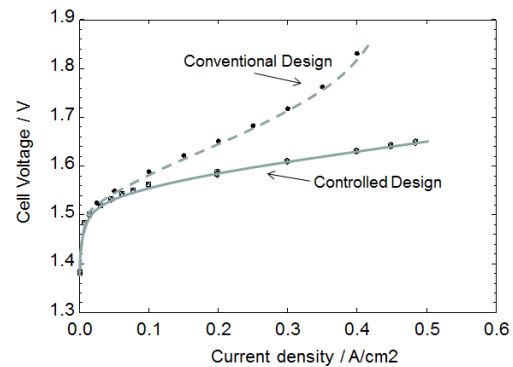**Fig. 1** Flow diagram of cathode feed SPE water electrolysis

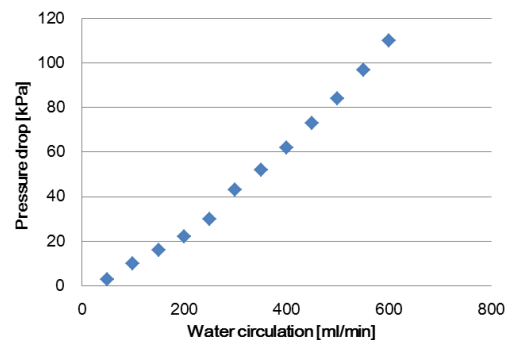**Fig. 2** I-V curve during the cathode-feed water electrolysis

Fig. 3 Pressure drop of water/gas separator